ISSN 0915-633X

NATIONAL INSTITUTE FOR FUSION SCIENCE

Analysis of Structure and Transition of Radial Electric Field in Helical Systems

S. Toda and K. Itoh

(Received - Feb. 16, 2001)

NIFS-686 Mar. 2001

RESEARCH REPORT
NIFS Series

TOKI, JAPAN

Analysis of structure and transition of radial electric field in helical systems

S. Toda and K. Itoh

National Institute for Fusion Science, Oroshi-cho 322-6, Toki 509-5292, Japan

E-mail: toda@ms.nifs.ac.jp

Abstract. A set of transport equations is analyzed, including the bifurcation of the radial electric field in toroidal helical systems. Calculations are made simulating CHS experiments. Both hard and soft transitions are found in the profile of the radial electric field. Whether the electric domain interface exists or not is examined. The electric domain interface is found to exist, depending on the ratio of the electron temperature to the ion temperature. The structure of the electric domain interface is also studied. The steep gradient of the radial electric field is obtained and the width of the electric domain interface is determined by the anomalous diffusivity of the electric field. The region where the electron root and ion root co-exist is obtained when changing the density or the heating power of electrons. The various types of the electrostatic potential structures are found. The condition for the turbulence suppression is examined in the parameter regime studied here.

KEYWORDS: radial electric field, neoclassical transport, anomalous transport, transport barrier, turbulence suppression

1. Introduction

Many types of the improved confinement states have been found in toroidal plasmas. (See reviews, *e.g.*, [1, 2, 3].) Among the variety of the improved confinement states, the H-mode in tokamaks has been studied most intensively. The bifurcation models of the electric field have been proposed to explain the physics of the H-mode transition and the L/H transition. [4, 5] Through evolution of research, it is widely recognized that the structure of the radial electric field influences on the various improved confinement modes. Nevertheless, quantitative analysis of the generation and the structure of the radial electric field in such plasmas is far from satisfactory. The investigation of the confinement improvement mechanisms has also been done for the helical plasmas.[6] The formation of the radial electric field in helical systems could be investigated more quantitatively, because the neoclassical transport is found to play the dominant roles in generating the radial electric field. (See, *e.g.*, [7, 8])

Recently, the internal transport barrier has been found in the Electron Cyclotron Resonance Heating (ECRH) plasma in CHS device. [9, 10, 11] The various types of the potentials have been obtained. In W7-AS, the studies of the change of the electron transport triggered by the neoclassical transport has been also done theoretically [12] and experimentally [13, 14]. More recently, the change of the anomalous transport in the central region has also been reported in W7-AS. [15] To study the existence of the transport barrier in the experimental conditions of helical plasmas, the investigation of the electric field bifurcation is needed. The interface of domains with different electric field polarities has been pointed out theoretically for helical plasmas. [16] It is well known that the neoclassical transport is dominant in the bipolar part of the particle flux in helical plasmas and the multiple solutions of the ambipolar condition are allowed. [8] In addition, there is the difference between the bifurcations under the fixed-gradient condition and the fixed-flux condition.[7] Dynamics and structure of the transport barrier have been examined by use of the analytical model. [17, 18, 19] The internal transport barrier in heliotron plasmas, which is induced due to the electric field bifurcation, was theoretically studied based on the zero-dimensional model. [20, 21] To study the interface of neighboring domains with different electric polarity, the one-dimensional transport analysis is needed. The possibility for the transport barriers (the edge transport barrier and the internal transport barrier) has been discussed based on the bifurcation model of the electric field; We have examined a set of one-dimensional transport equations which constitute the temporal evolution of the temperature and the diffusion equation the radial electric field in a slab plasma. [22] However, this study is limited within the analysis in the edge region and the studies of the internal transport barrier in the central region are needed.

In this article, we examine the four (one-dimensional) transport equations which describe the temporal evolutions of the density, the electron and ion temperatures, and the radial electric field in a cylindrical heliotron configuration to examine the detailed structure and the dynamics of the electric domain quantitatively. A numerical

formula [23] for the non-axisymmetric part of the neoclassical flux is adapted. The electric field domain is studied in helical plasmas. The anomalous transport process is assumed to be ambipolar, because the electric field formation due to the neoclassical transport is considered to be dominant compared to that due to the anomalous transport [19, 24]. This is confirmed by the present observations in experiments. [11] The impact of the possible bipolar part of the anomalous transport will be studied in the future study. Various types of potentials are reproduced, depending on the value of density and the ratio of the ion temperature to the electron temperature. We study the radial profile of the electric field and examine the states in which the electric domain exists. We also show the condition for the hard transition where the flux is the continuous function of the plasma radius. The hard type transition is accompanied by the temporal and/or spatial rapid change of the radial electric field when the multiple solutions of the ambipolar condition exist. The states which associate with the internal transport barrier are studied in the profile of the temperature. The soft transition occurs with the temporal and/or spatial slow change of the radial electric field when only one solution exists. The effect of the inertia with the temporal change of the heating power on the location of the electric domain is examined. We compare the structures of the potentials in the case of the soft and hard transitions. Finally, we discuss the condition of the turbulence suppression.

2. One-dimensional Model Equations

In this section, the model equations used here are shown. The cylindrical coordinate is used and r-axis is taken in the radial cylindrical plasma in this article. The region $0 \leq r \leq a$ is considered, where a is the minor radius. The expression for the radial neoclassical flux associated with helical-rippled trapped particle is given as [23]

$$\Gamma_j^{na} = -\epsilon_t^2 \sqrt{\epsilon_h} v_{dj}^2 n_j \int_0^\infty dx x^{\frac{5}{2}} e^{-x} \tilde{\nu}_j \frac{A_j(x, E_r)}{\omega_j^2(x, E_r)}, \tag{1}$$

where $x \equiv m_j v^2/(2T_j)$, $A_j(x, E_r) = n_j'/n_j - Z_j e E_r/T_j + (x - 3/2)T_j'/T_j$, $\omega_j^2(x, E_r) = 3\tilde{\nu}_j^2(x) + 1.67(\epsilon_t/\epsilon_h)(\omega_E + \omega_{Bj})^2 + (\epsilon_t/\epsilon_h)^{\frac{3}{2}}\omega_{Bj}^2/4 + 0.6\,|\omega_{Bj}|\,\tilde{\nu}_j$ and $\tilde{\nu}_j(x) = \nu_{thj}/(\epsilon_h x^{\frac{3}{2}})$. Here, the relations $\omega_E = -E_r/(rB)$, $\omega_{Bj} = -T_j \epsilon_h' x/(Z_j e r B)$ and $v_{dj} = -T_j/(Z_j e r B)$ are used. The quantities m_j, n_j, T_j, ν_{thj} are the mass, the density, the temperature, the collision frequency using the thermal velocity for the species j and the parameters ϵ_t and ϵ_h are the toroidal and helical ripple, respectively. The prime denotes the derivative with respect to the radial direction. This expression for the particle flux is the connection formula and is applicable to both the collisionless and collisional regimes. The total particle flux Γ^t is written as

$$\Gamma^t = \Gamma^{na} - D_a \frac{\partial n}{\partial r}. \tag{2}$$

Here, D_a is the anomalous component of the particle diffusivity. The energy flux related with neoclassical ripple transport is given as [23]

$$Q_j^{na} = q_j^{na} + \frac{5}{2}\Gamma_j^{na}T_j = -\epsilon_t^2\sqrt{\epsilon_h}\nu_{dj}^2 n_j T_j \int_0^\infty dx x^{\frac{7}{2}} e^{-x}\tilde{\nu}_j(x)\frac{A_j(x,E_r)}{\omega_j^2(x,E_r)}. \quad (3)$$

The total heat flux Q_j^t of the species j is written as

$$Q_j^t = Q_j^{na} - n\chi_{aj}\frac{\partial T_j}{\partial r}. \quad (4)$$

Here, χ_{aj} is the anomalous part of the heat conductivity for the species j. The neoclassical component of the diffusion coefficient for the electric field is expressed by [25]

$$D_{E_j} = -\frac{e}{\epsilon_\perp}\frac{3}{16\sqrt{2\pi}}\frac{Z_j e}{T_j}\frac{n_j\nu_{thj}T_j^4}{(Z_j e)^4}\frac{\epsilon_t^4}{\sqrt{\epsilon_h}}\left(1+\frac{\epsilon_t}{\epsilon_h}\right)\int_{x_b}^\infty \frac{dxe^{-x}x^3}{\left(|E_r| + \left|x\frac{T_j}{Z_j e}\epsilon_h'\right|\right)^4}, \quad (5)$$

where $x_b = [\nu_{thj}/(\epsilon_h(|E_r| + |T_j/(Z_j e)\epsilon_h'|))]^{2/3}$. The parameter used later D_{Ea} is the anomalous component of the diffusion coefficient for the radial electric field. In this article, the coefficients for the anomalous transport are set to be constant. This simplification is introduced because the structure of the electric domain interface is the primary interest of this article. As is shown in the following analysis, the domain interface has much shorter scale length than the global scale length. The interactions between the anomalous transport and the inhomogeneity of the electric field are not subject of this article.

The equation for the density is

$$\frac{\partial n}{\partial t} = -\frac{1}{r}\frac{\partial}{\partial r}(r\Gamma^t) + S_n. \quad (6)$$

The term S_n represents the particle source such as the ionization effect. The equation for the electron temperature is given as

$$\frac{3}{2}\frac{\partial}{\partial t}(nT_e) = -\frac{1}{r}\frac{\partial}{\partial r}(rQ_e^t) - \frac{m_e}{m_i}\frac{n}{\tau_e}(T_e - T_i) + P_{he}, \quad (7)$$

where, the term τ_e denotes the electron collision time and the second term in the right hand side represents the heat exchange between ions and electrons. The parameter P_{he} represents the absorbed power due to the ECRH heating and its profile is assumed to be proportional to $\exp(-(r/(0.2a))^2)$ for simplicity. The equation for the ion temperature is

$$\frac{3}{2}\frac{\partial}{\partial t}(nT_i) = -\frac{1}{r}\frac{\partial}{\partial r}(rQ_i^t) + \frac{m_e}{m_i}\frac{n}{\tau_e}(T_e - T_i) + P_{hi}. \quad (8)$$

The parameter P_{hi} represents the absorbed power of ions and its profile is also assumed to be proportional to $\exp(-(r/(0.2a))^2)$.

The radial electric field equation in a nonaxisymmetric system is expressed by [25]

$$\frac{\partial E_r}{\partial t} = -\frac{e}{\epsilon_\perp}\sum_j Z_j\Gamma_j^{na} + \frac{1}{r}\frac{\partial}{\partial r}\left(\sum_j Z_j(D_{Ej} + D_{Ea})r\frac{\partial E_r}{\partial r}\right), \quad (9)$$

where $\epsilon_\perp$ is the perpendicular dielectric coefficient as $\epsilon_\perp = \epsilon_0((c^2/v_A^2)+1)(1+2q^2)$. Here, ϵ_0 is the dielectric constant in the vacuum, c is the speed of light, v_A is the velocity of

Alfvén wave and q is the safety factor. The parameter Z_j is a charge number of the species j. The factor $(1+2q^2)$ is introduced from the toroidal effect.[19, 24] Equation (9) is solved together with the density and the temperature (ion and electron) equations (6), (7) and (8).

3. Results of Analysis

3.1. Boundary conditions and Parameters

The density, temperature and electric field equations (6), (7), (8) and (9) are solved under the appropriate boundary conditions. For the initial condition, we choose $E_r(r) \equiv 0$ and the plasma profiles evolve to the steady state. We fix the boundary condition at the center of plasma ($r = 0$) such as $\partial n/\partial r = \partial T_e/\partial r = \partial T_i/\partial r = E_r(= -\partial\phi/\partial r) = 0$, where ϕ is the electrostatic potential of the radial electric field. For the diffusion equation of the radial electric field, equation (9), the boundary condition at the edge ($r = a$) is chosen as $\sum_j Z_j\Gamma_j = 0$. This implies that there is no divergence of the flux at the plasma surface. This simplified assumption is employed because the electric field bifurcation in the core plasma is the main subject of this article. The boundary conditions at the edge ($r = a$) with respect to the density and the temperature are those expected in Compact Helical System (CHS): $-n/n' = 0.05(m)$ and $-T_e/T_e' = -T_i/T_i' = 0.02(m)$. The machine parameters are those of the CHS device, such as the major radius $R = 1(m)$, $a = 0.2(m)$, the toroidal magnetic field $B = 1(T)$, toroidal mode number $m = 8$, poloidal mode number $l = 2$ and helical ripple $\epsilon_h(r) = lCI_l(mr/R)$, where I_l is the modified Bessel function of the first kind and the typical value of C is chosen according to the experimental condition.

The particle source term S_n is assumed to be $S_n = S_0\exp((r-a)/L_0)$, where L_0 is set to be $100(m)$ and the value of S_0 is strongly influenced by the particle confinement time. If these parameters are used, we can study the case $\bar{n} \simeq 10^{18}(m^{-3})$, when the value of S_0 is set to be $S_0 = 10^{23}(m^{-3}s^{-1})$. Here, $\bar{n}$ is the averaged density. For simplicity, the enhancement factor of flow inertia owing to the toroidal effect is chosen as $(1 + 2q^2) = 10$. The values for the anomalous parts of the diffusion coefficients are chosen as $D_a = 1(m^2/s)$, $\chi_{ae} = 5(m^2/s)$ and $\chi_{ai} = 1(m^2/s)$. The value of D_{Ea} is $D_{Ea} = 10(m^2/s)$. They do not necessarily coincide those in experiments. This simplification is employed to illustrate the existence of the electric field interface in CHS plasmas. These values are set to be constant spatially and temporally. In order to set averaged temperature of electrons to be around $\bar{T}_e = 200(eV)$ and the density to be around $\bar{n} = 10^{18}(m^{-3})$, the absorbed power of electrons is around $10kW$, for this choice of χ_{ae}. The averaged ion temperature $\bar{T}_i$ is chosen as about $\bar{T}_i = 400(eV)$, where the absorbed power of ions is fixed as $6.25(kW)$. These values of the absorbed power are determined by the values of the anomalous diffusivities.

3.2. Solutions with the Hard Transition

Using these parameters and the boundary conditions, we analyze equations (6), (7), (8) and (9). The stationary solutions of the radial electric field are shown in figure 1(a) for the case of $\bar{T}_e = 130(eV)$, $\bar{T}_i = 400(eV)$ and $\bar{n} = 1.4 \times 10^{18}(m^{-3})$. The density profile and the temperature profile of the ion and the electron are shown in figures 1(b) and (c), respectively. In figure 1(c), the dashed line represents the case of the ion temperature and the solid line shows the profile the electron temperature. At the point $r = r_T$($0.08(m)$), the transition of the radial electric field is found. The circles in figure 1(a) show the values of the electric field which satisfy the local ambipolar condition ($\Gamma_e^{na} = \Gamma_i^{na}$) for the calculated profiles of the density and the temperatures of figures 1(b) and (c). The multiple solutions are allowed from the local ambipolar condition. The electron root and ion root are defined in this article as follows: We call the solution the electron root if it is in the region of $\partial\Gamma_i^{na}/\partial E_r < 0$ and the ion root if $\partial\Gamma_i^{na}/\partial E_r > 0$, respectively. In the case of figure 1(a), the electron root ($r < r_T$) for E_r is sharply connected to the ion root ($r > r_T$), with the thin layer between them. At the transition point ($r = r_T$), the maximum value of the electric field shear $|E_r'|$ is found to appear. In figure 2, the profile of the derivative of the radial electric field is shown. The peak of dE_r/dr at the transition point $r = r_T$ is found. In the present model, the effect of the anomalous transport does not play any role in generating the radial electric field, because it is assumed to be ambipolar. However, the anomalous transport influences the width of the domain interface. The half width of the peak in the profile of the radial electric field shear is proportional to $\sqrt{D_{E_a}}$ and the value of the peak of the electric field shear is proportional to $D_{E_a}^{-1/2}$. The transition points should be determined by the Maxwell construction.[19] The function

$$\Delta\Psi = \int_{E_1}^{E_2} (\Gamma_i^{na}(E_r) - \Gamma_e^{na}(E_r))dE_r \tag{10}$$

is introduced, where E_1 and E_2 are the stable solutions of the local ambipolar condition. The integral $\Delta\Psi$ is a function of the radius. The relation $\Delta\Psi = 0$ at the domain interface $r = r_T$ represents the Maxwell construction. We confirm that the Maxwell construction is satisfied in the case of figure 1. It is found that there is the difference between the half widths at the half maximum of the inner side ($r < r_T$) and the outer side ($r > r_T$) in the profile of the electric field shear. The half width of the inner side is wider than that of the outer side due to the dependence of the current on the radial electric field. The origin of this asymmetry is discussed in the reference [26].

It is also noted that in this steady state the radial fluxes for the particles and the energy are continuous across the domain interface $r = r_T$. The continuity of flux leads to the steep change of the gradients. Note that the change of the radial electric field is obtained in spite of using the large value for the anomalous diffusivity, *i.e.*, $D_{E_a} = 10(m^2/s)$, which is a typical value of the plasmas in CHS plasmas. In figures 1(b) and 1(c), the gradients of the density and the temperatures rapidly changes at the transition point ($r = r_T$). Therefore, the profile of the local ambipolar solution

of the electric field (figure 1(a)) is also sharply modulated near the transition point ($r \approx r_T$). This calculation in the flux-fixed case is the difference with the calculation in the case of the fixed gradients.

The internal transport barrier is obtained for the channel of the neoclassical energy transport, being observed in the both the ion and electron temperature profiles in figure 1(c). In figure 3, the variations of the neoclassical part χ_j^{na} of the heat conductivity for the species j are shown. At the transition point, the rapid change of both χ_e^{na} and χ_i^{na} is obtained. Within the radius of $r \leq r_T$, the neoclassical transport is reduced and the transport barrier is obtained. This corresponds to the rapid change of ∇T_e and ∇T_i at $r = r_T$ in figure 1(c). The steeper gradient is observed in the ion temperature profile than in the electron temperature profile in this case. This is because the value of χ_{ae} larger than the value of χ_{ai} is chosen.

The existence and the location of the electric domain interface depend on the plasma parameters. Figure 4 shows the change of the regions of the electron root and the ion root as a function of the electron temperature. The series of the stationary state is calculated when the averaged temperature of the electrons takes the value from $50(eV)$ to $600(eV)$, by changing P_{he}. Other parameters are same as the previous analysis. The electric domain exists at the solid line in figure 4. The electron root and the ion root are neighboring where the solid line exists. The heating power P_i of ions is fixed and the averaged ion temperature $\bar{T}_i$ is set to be around $400(eV)$. When the averaged temperature of electrons is low, solutions in the whole plasma column are ion roots. On the other hand, all solutions become electron roots if the averaged temperature of electrons increases up to $600(eV)$. The parameter regime ($300(eV) < \bar{T}_e < 600(eV)$) is found where the electron root exists in the inner region and the ion root exists in the outer region. In the region of $80(eV) < \bar{T}_e < 600(eV)$, the central and edge plasmas are associated with the ion root solution and two domain interfaces exist in a plasma simultaneously.

The region of the electron root expands when the electron density becomes lower. Figure 5 shows the relation between the values of the density and the temperature of electron at $r/a = 0.5$ in the stationary state. The averaged value of the density changes by changing the value of particle source S_0. We fix the ion heating power $6.25(kW)$ and the averaged ion temperature $\bar{T}_i$ is set to be around $400(eV)$. The averaged value of the electron temperature $\bar{T}_e$ takes the value from $100(eV)$ to $400(eV)$. Other parameters are same as the previous analyses. If the density takes the larger value, the E_r solution changes from the electron root and the ion root and the electric domain passes through at some value of the density. The discontinuity in the relation between $n(r/a = 0.5)$ and $T_e(r/a = 0.5)$ due to the hard transition is seen around the parameter regime $n(r/a = 0.5) \approx 1.32 \times 10^{18}(m^{-3})$ as shown by the arrow in figure 5. It is found that the electric domain interface moves from the outer region to the inner region when the density increases, and the electric domain interface moves across the point $r/a = 0.5$ when the value of the density becomes $n(r/a = 0.5) \approx 1.32 \times 10^{18}(m^{-3})$.

3.3. Dynamical (Inertia) Effect

When the plasma parameter changes in time, the radial electric field shows the temporal evolution. If the temporal change is fast, the inertial term in equation (9) influences the radial profile of the electric field. The change of the location of the electric domain interface is studied when the heating power of electrons increases or decreases.

At first, the case of the ramp-down of the electron heating is examined. The change of the location of the electric domain interface is shown when the averaged temperature of electrons becomes lower from $500(eV)$ to $50(eV)$ with the dashed line in figure 6. Other parameters are same as the analysis in the previous subsection. The time during which $\bar{T}_e$ temporally changes from $500(eV)$ to $50(eV)$ is $0.5(s)$. This time is about one hundred times longer than the typical confinement time ($a^2/D_{E_a} = 4(ms)$). Note that the profile of the physical quantity is not stationary in the case of figure 6, when we judge whether the solution is the electron root or the ion root. The so-called inertia effect (the time derivative of the physical quantities) is included. The location of the radial electric domain interface is found to be altered due to the inertia effect when, *e.g.*, the heating power changes. If the averaged temperature of electrons temporally decreases, the region of the electron root gets wider compared to the case of the stationary state. Under this slow change in time, the electric domain interface is influenced little except in the central region ($r/a \leq 0.2$).

Secondly, we study the case of the ramp-up of the electron heating power. The change of the location of the electric domain interface is shown when the averaged temperature of electrons becomes higher from $500(eV)$ to $50(eV)$ with the dotted line in figure 6. The time during during which $\bar{T}_e$ temporally changes from $150(eV)$ to $600(eV)$ is also $0.5(s)$. If the averaged temperature of electrons temporally becomes higher, the electric domain interface moves to the higher region of the averaged electron temperature compared to the stationary state.

There is the difference of the location of the transition point between the two cases when the heating power increases and decreases. The hysteresis characteristic is predicted in the case when the heating power increases after it decreases. In fact, the experimental results show the hysteresis characteristic in the relation the heat flux and the gradient of the electron temperature when the heating power is ramped down and ramped back up again. [15]

3.4. Solutions with the soft transition

We next study the case where the soft transition between the ion and electron roots takes place. We choose the case that the ion heating vanishes, *i.e.*, $P_{hi} = 0$ in order to study the case when the electron temperature in much higher than the ion temperature. We set the electron heating is $100(kW)$ and the particle source term $S_0 = 9 \times 10^{23}$. The averaged density is set to be around $1.4 \times 10^{19}(m^{-3})$. The other parameters are same as the previous case in which the hard transition is seen in figure 1. The obtained profiles of the density, the temperature and the radial electric field are shown in figure 7. In

figure 7(c), the solid line represents the case of the electron temperature and the dashed line shows the profile the ion temperature. In figure 7(a), the radial profile of the electric field is shown, obtaining the soft transition without the multiple solutions. The electron root and the ion root connect smoothly and the electric domain interface does not exist in this case of the soft transition. The arrow in figure 7(a) shows the radial point ($r = 0.078(m)$) across which the solution changes from the electron root ($r < 0.078(m)$) to the ion root ($r > 0.078(m)$) in the radial direction. The type of the transition (hard or soft) is determined by the ratio T_e/T_i, and does not depend on the diffusion coefficient D_{E_a} of the radial electric field. The gradient of E_r at the transition point is much weaker than the case of figure 1. The gradient is in the range of $|E_r'| \leq 10^5$ near $r = r_T$, where the maximum value of $|E_r'|$ takes at $r = r_T$. In the parameter region examined here, the slow change of the temperature is found and the state which corresponds to the internal transport barrier is not obtained in figure 7(c). In figure 8, the relation between the values of the density and the temperature of the electrons at $r/a = 0.5$ is illustrated. The solutions are obtained in the stationary state with the electron heating $100kW$, no ion heating and the particle source S_0 takes various values so as to change the averaged value of the density $\bar{n}$. The smooth connection from electron root to the ion root is obtained, when the averaged density increases due to the characteristic of the soft transition. The value for the averaged density where the solution changes from the electron root to ion root is dictated by the arrow and is about $1.23 \times 10^{19}(m^{-3})$ in the parameter regime examined here.

4. Varieties of Potential Profiles

In experiments in CHS, the various types of electrostatic potentials are observed. These potential are classified to many shapes, *e.g.*, bell-shape, dome-shape, hill-shape, Mexican hat-shape and well-shape. [11] In the previous section, we show the cases where the hard and soft transition take place. We show the each profile of the potential in the case of the hard or soft transition. The values of the anomalous transport coefficients are same as the previous section.

At first, in the case of the hard transition, the particle source S_0 is set as $S_0 = 1 \times 10^{23}$ (averaged density is around $10^{18}(m^{-3})$) and the ion heating power is $6.25(kW)$. If the averaged temperature of electrons is low ($80(eV)$ in figure 9), the shape of the potential has a single minimum at $r = 0$ and looks like well-shape. When the averaged temperature of electrons increases ($130(eV)$ as is discussed in the previous section in figure 9), the electric domain interface appears at $r = r_T$. The potential looks like Mexican hat-shape in figure 9. The steep change of E_r or the large E_r shear is obtained at $r = r_T(\approx 0.08(m))$, because the hard transition occurs at this point. The corner of the curve of the potential at $r = r_T$ is very sharp. In this case, the electric domain is found to exist. If the averaged temperature of electrons increases up to $600(eV)$, the potential has a single maximum at $r = 0$ and looks like hill.

As the second case, we examine the case of the no ion heating $P_i = 0$ and $T_e >> T_i$

holds. The heating power of electrons is chosen as $100(kW)$. In this study, we study the change of the radial electric field structure which is induced by the variation of the density. In figure 10, we choose the various values for the particle source term. In the case when the averaged density is high (*e.g.*, $3.2 \times 10^{19}(m^{-3})$ in figure 10), the shape of the potential looks like well-shape. When the averaged density is the intermediate value, $1.6 \times 10^{19}(m^{-3})$, the potential looks like Mexican hat-shape. The polarity of the radial electric field changes at $r \approx 0.08(m)$. The slow change of the radial electric field is obtained and the electric domain does not exist. If the averaged density decreases up to $1.5 \times 10^{18}(m^{-3})$, the potential shape looks like hill. If the ion is not heated and T_i is much lower than T_e, the type of the transition becomes soft. In this case, the multiple solutions are not seen and the change from the electron root to the ion root becomes smooth. Therefore, the large E_r shear is not obtained when the ion is not heated like the case in figure 10. Compared with the both cases of the Mexican hat-shape in figure 9 and figure 10, whether the electric domain exists or not is the main difference. Only in the case of the hard transition, the sharp change of the electric field is obtained.

5. Condition for Turbulence Suppression

A important model for reducing turbulent transport, *e.g.*, in the H-mode transport barrier in tokamaks is based on the sheared radial electric field. A nonlinear current diffusive interchange instability can be stabilized when $|E_r'/B| > (\sqrt{r/R})sC_s/a$, where C_s is the sound speed and s is the magnetic shear. [6] At the transition point $r = r_T$ in figure 1, this condition is marginal. Therefore, the anomalous diffusivities are suppressed if the turbulent model is used for the anomalous diffusivities. The self-consistent analysis, in which the change of the anomalous transport by the electric field shear E_r' is included, is necessary and is left for the future study.

6. Summary and Discussions

In summary, the model equation of the radial electric field bifurcation is analyzed. We studied the temporal and spatial evolutions of the plasma density, the temperatures and the radial electric field. The numerical formula of the neoclassical components of particle and heat fluxes in helical systems is employed.

The stationary structure of the radial electric field is examined and the hard-type transition with hysteresis characteristic is newly found in heliotron plasmas. The structure of the electric domain is studied. The state which corresponds to the internal transport barrier is obtained in the radial structures of the temperatures and the heat conductivities. The profiles of the physical quantities are also shown in the case of the soft transition from the electron root to the ion root in the radial direction. The classification whether the solution in the stationary state is the electron root or the ion root is done based on the sign of $\partial\Gamma_i^{na}/\partial E_r$. It is found that the electron root and ion root can co-exist in a plasma column. The states where the hard and soft transitions

occur are compared and obtained, depending on the ratio T_i/T_e. The relation between the density and the temperature in the stationary state is studied in both cases when the hard transition or soft transition takes place. In the case when the hard transition happens, the electric domain interface appears, across which the steep gradients of the density, the temperature and the electric field appear. The effect of the temporal change of the heating power on the location of the electric domain is also examined. The electrostatic potential profiles are also shown in the both cases when the hard or soft transition occurs. At last, the condition for the turbulence suppression is studied at the point where the hard transition occurs.

In this article, we set the anomalous diffusivities (D_a, χ_{aj} and D_{Ea}) to be constant, temporally and spatially. To compare the experimental results in details, the calculation by use of the turbulent model with respect to the anomalous diffusivities is needed. The results of the calculations using the turbulence suppression model are not shown in this article. These are left for future studies.

Acknowledgments

Authors would like to acknowledge Prof. S. -I. Itoh, Prof. A. Fukuyama and Dr. M. Yagi for illuminating discussion on the problem. In particular, one of the authors (ST) thanks Prof. A. Fukuyama for the helpful suggestions in numerical methods. Discussions with Dr. A. Fujisawa and Dr. H. Sanuki are also acknowledged. This work is partly supported by Grant-in-Aid for Scientific Research on Ministry of Education, Culture, Sports, Science and Technology of Japan.

References

[1] Itoh K and Itoh S -I 1996 Plasma Phys. Control. Fusion **38** 1
[2] Burrell K H 1997 Phys. Plasmas **4** 1499
[3] Connor J W and Wilson H R 2000 Plasma Phys. Control. Fusion **42** 1
[4] Itoh S -I and Itoh K 1988 Phy. Rev. Lett.**60** 2278
[5] Shaing K C and Crume E C Jr. 1989 Phy. Rev. Lett.**63** 2369
[6] Itoh K, Itoh S -I, Fukuyama A, Sanuki H and Yagi M 1994 Plasma Phys. Control. Fusion **34** 123
[7] Kovrizhnykh L M 1984 Nucl. Fusion **24** 851
[8] Ida K 1998 Plasma Phys. Control. Fusion **40** 1429
[9] Fujisawa A *et al* 1997 Phys. Rev. Lett. **79** 1054
[10] Fujisawa A *et al* 1999 Phys. Rev. Lett. **82** 2669
[11] Fujisawa A *et al* 2000 Phys. Plasmas **7** 4152
[12] Maaßberg H, Brackel R, Burhenn R, Gasparino U, Grigull P, Kick M, Kühner G, Ringer H, Sardei F, Stroth U and Weller A 1993 Plasma Phys. Control. Fusion **35** B319
[13] Kick M, Maaßberg H, Anton M, Baldzuhn J, Endler M, Görner C, Hirsch M, Weller A, Zoletnik S and the W7-AS Team 1999 Plasma Phys. Control. Fusion **41** A549
[14] Maaßberg H, Beidler C D, Gasparino U, Romé, the W7-AS Team, Dyabilin K S, Marushchenko N B and Murakami S 2000 Phys.Plasmas **7** 295
[15] U. Stroth *11th Toki International Conference on Plasma Physics and Controlled Nuclear Fusion* (ITC-11) 2000 **III-4**.
[16] Hastings D E, Houlberg W A and Shaing K C 1985 Nucl. Fusion **25** 445
[17] Diamond P H, Lebedev V B, Newman D E and Carreras B A 1995 Phys. Plasmas **2** 3685
[18] Diamond P H, Lebedev V B, Newman D E, Carreras B A, Hahm T S, Tang W M, Rewoldt G and Avinash K 1997 Phys. Rev. Lett. **78** 1472
[19] Itoh K, Itoh S -I and Fukuyama A 1999 *Transport and Structual Formation in Plasmas* (IOP, England, London, England, 1999), Chap. 12
[20] Itoh K, Sanuki H, Toda S, Itoh S -I, Yagi M and Fukuyama A 1999 *26th EPS Conf. on Control. Fusion and Plasma Phys. 14-18 June 1999, Maastricht, The Netherlands* 1309
[21] Sanuki H, Itoh K, Yokoyama M, Fujisawa A, Ida K, Toda S, Itoh S -I, Yagi M and Fukuyama A 2000 J. Phys. Soc. Jpn. **69** 445
[22] Toda S and Itoh K 2000 J. Plasma Fusion Res. SERIES Vol. **3** 580
[23] Shaing K C 1984 Phys. Fluids **27** 1567
[24] Hinton F L and Robertson J A 1984 Phys. Fluids **27** 1243
[25] Hasting D E 1985 Phys. Fluids **28** 334
[26] Itoh K, Sanuki H, Toda S, Yokoyama M, Itoh S -I, Yagi M and Fukuyama A 2000 *11th Toki International Conference on Plasma Physics and Controlled Nuclear Fusion* (ITC-11) **PII-20**

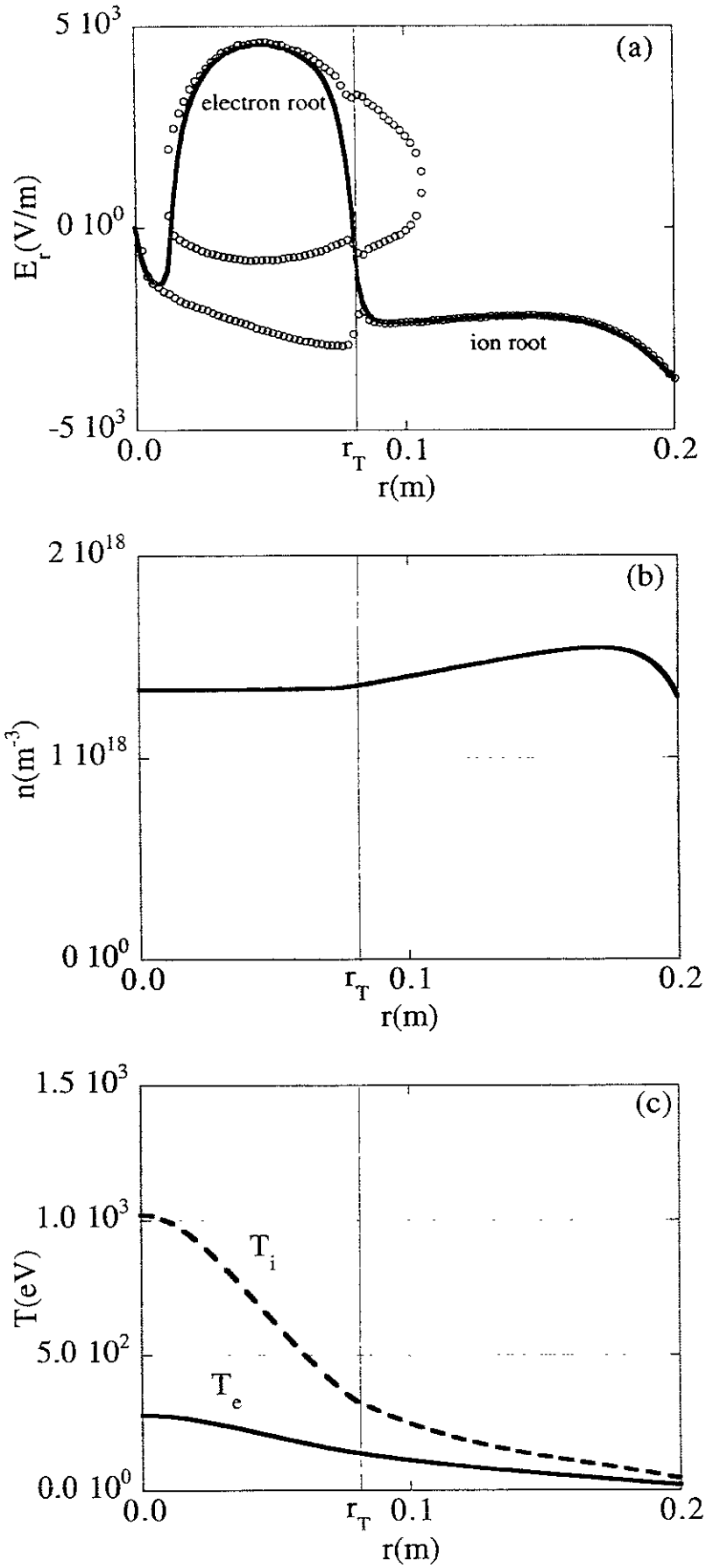

Figure 1. (a) Radial dependence of the electric field (Solid line). Circle marks show the electric field derived from the ambipolar condition. Radial profile of the density (b) and the profiles of the temperature of ions and electrons (c) are shown. Parameters are $D_a = 1(m^2/s)$, $\chi_{ae} = 5(m^2/s)$, $\chi_{ai} = 1(m^2/s)$ and $D_{E_a} = 10(m^2/s)$.

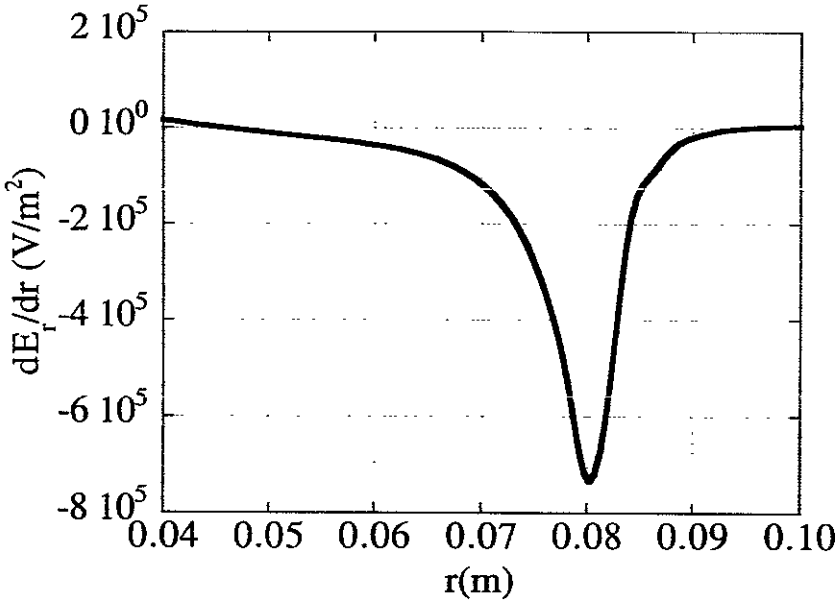

Figure 2. Radial variation for the derivative of the electric field. The peak at $r = r_T$ is found to be obtained.

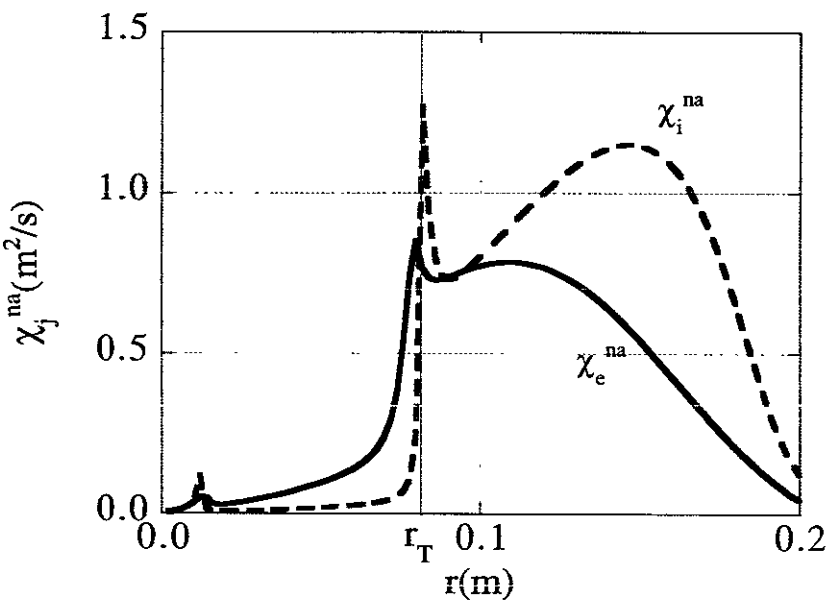

Figure 3. Radial profiles of the neoclassical heat conductivity of electrons (solid line) and ions (dashed line) for the case of figure 1.

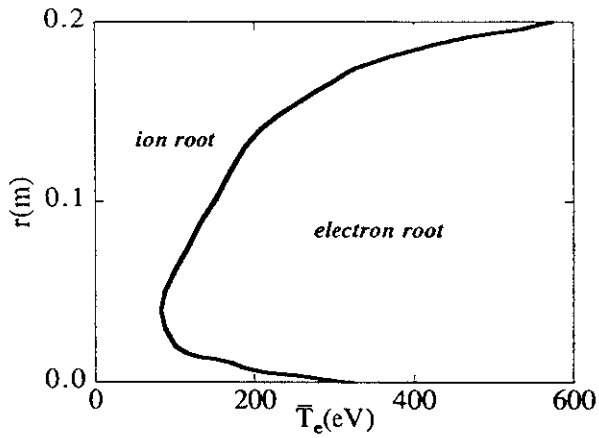

Figure 4. Location of the domain interface as a function of $\bar{T}_e$. The change of the radial regions of the electron root and the ion roots when the averaged temperature of electron takes the value from $50(eV)$ to $600(eV)$.

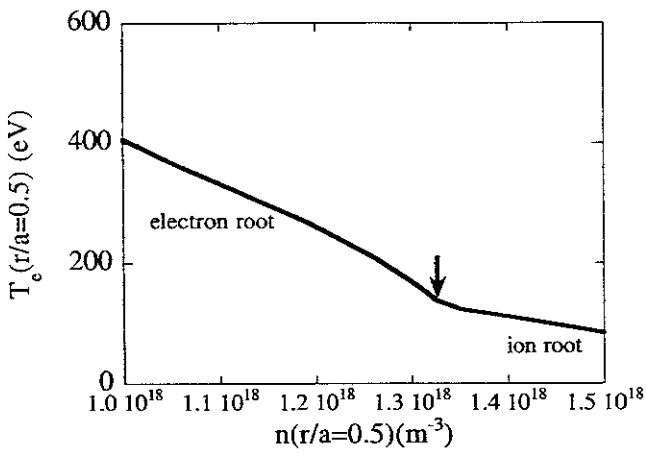

Figure 5. Contour line on the plane of the density and the temperature of the electrons at $r/a = 0.5$ in the stationary state with the ion heating The arrow represents the density value in which the radial electric field E_r changes from the electron root to the ion root.

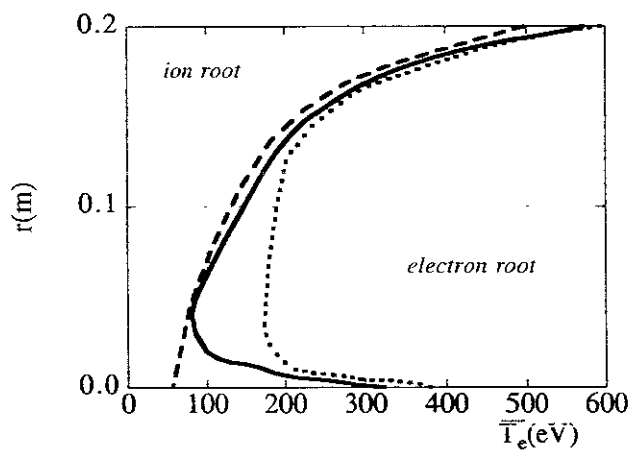

Figure 6. The change of the radial regions of the electron root and the ion roots when $\bar{T}_e$ temporally decreases from $500(eV)$ to $50(eV)$ is obtained with the dashed line. The change of the radial regions of the electron root and the ion roots when $\bar{T}_e$ increases from $150(eV)$ to $600(eV)$ is also obtained with the dotted line. The solid line represents the location of the electric domain obtained from the stationary state (same as figure 4).

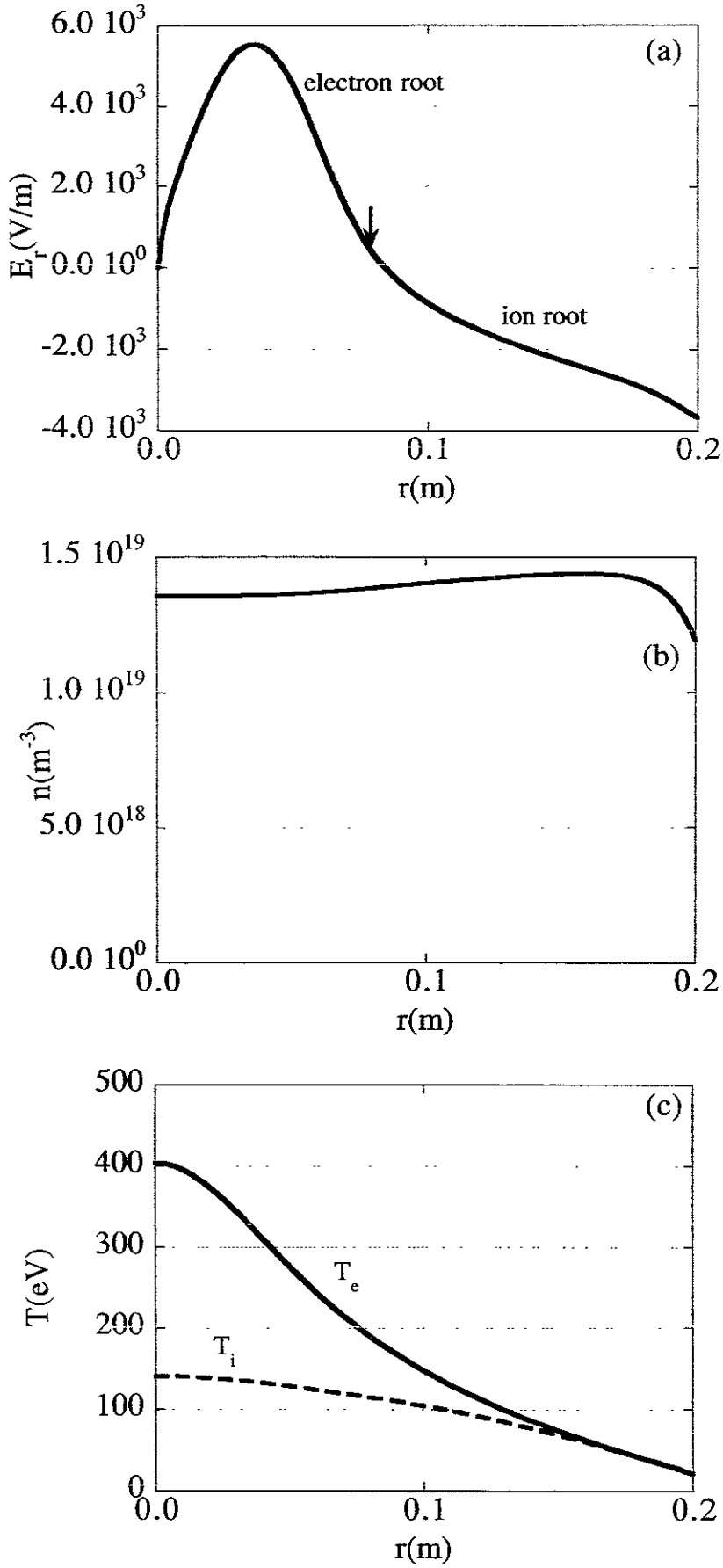

Figure 7. (a) Radial profile of the electric field is shown. The arrow shows the radial point ($r = 0.078(m)$) in which the solution smoothly changes from the electron root to the ion root. The particle source term is $S_0 = 9 \times 10^{23}$. Radial profile of the density (b) and the profiles of the temperature of ions and electrons (c) are shown.

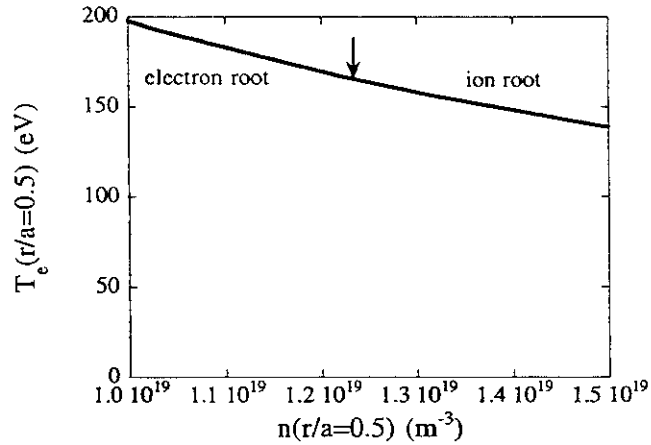

Figure 8. Contour line on the plane of the density and the temperature of the electrons at $r/a = 0.5$ in the stationary state with no ion heating. The slow change of the contour line is obtained. The arrow shows the values of the density ($1.23 \times 10^{19}(m^{-3})$) and the temperature ($160(eV)$) in which the solution changes from the electron root to the ion root.

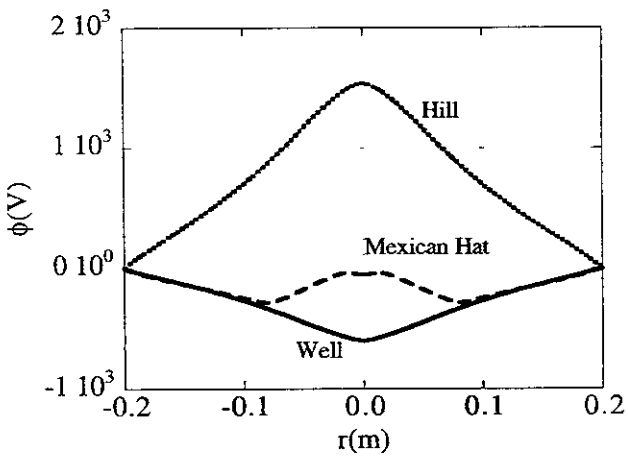

Figure 9. Change of the potential profiles with the absorbed power in the case of the hard transition. In the cases of the dotted (Hill), dashed (Mexican Hat), and solid (Well) lines, the averaged electron temperatures are $600eV$, $130eV$ and $80eV$, respectively.

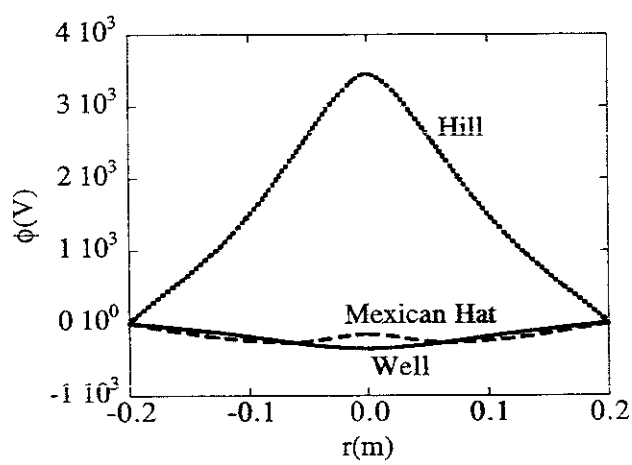

Figure 10. Change of the potential profiles with the particle source in the case of the soft transition In the cases of the dotted (Hill), dashed (Mexican Hat), and solid (Well) lines, the averaged densities are $1.5 \times 10^{18}(m^{-3})$, $1.6 \times 10^{19}(m^{-3})$ and $3.2 \times 10^{19}(m^{-3})$, respectively

Recent Issues of NIFS Series

NIFS-662 T Hayashi, N Mizuguchi, H Miura and T Sato,
Dynamics of Relaxation Phenomena in Spherical Tokamak Sep 2000
(IAEA-CN-77THP2/13)

NIFS-663 H Nakamura and T Sato H Kambe and K Sawada and T Saiki,
Design and Optimization of Tapered Structure of Near-field Fiber Probe Based on FDTD Simulation Oct 2000

NIFS-664 N Nakajima,
Three Dimensional Ideal MHD Stability Analysis in $L=2$ Heliotron Systems Oct 2000

NIFS-665 S Fujiwara and T Sato,
Structure Formation of a Single Polymer Chain I Growth of trans Domains Nov 2000

NIFS-666 S Kida,
Vortical Structure of Turbulence Nov 2000

NIFS-667 H Nakamura, S Fujiwara and T Sato,
Rigidity of Orientationally Ordered Domains of Short Chain Molecules Nov 2000

NIFS-668 T Mutoh, R Kumazawa, T Seki, K Saito, Y Torii, F Shimpo, G Nomura, T Watari, D A Hartmann, M Yokota, K Akaishi, N Ashikawa, P deVries, M Emoto, H Funaba, M Goto, K Ida, H Idei, K Ikeda, S Inagaki, N Inoue, M Isobe, O Kaneko, K Kawahata, A Komori, T Kobuchi, S Kubo, S Masuzaki, T Morisaki, S Morita, J Miyazawa, S Murakami, T Minami, S Muto, Y Nagayama, Y Nakamura, H Nakanishi, K. Narihara, N Noda, K Nishimura, K Ohkubo, N Ohyabu, S Ohdachi, Y Oka, M Osakabe, T Ozaki, B J Peterson, A Sagara, N Sato, S Sakakibara, R Sakamoto, H Sasao M Sasao, M. Sato, T Shimozuma, M Shoji, S Sudo, H Suzuki, Y Takeiri, K Tanaka, K Toi, T Tokuzawa, K Tsumori, K Y Watanabe, T Watanabe, H Yamada, I Yamada, S Yamaguchi, K Yamazaki, M Yokoyama, Y Yoshimura, Y Hamada, O Motojima, M Fujiwara,
Fast- and Slow-Wave Heating of Ion Cyclotron Range of Frequencies in the Large Helical Device. Nov 2000

NIFS-669 K Mima, M.S Jovanovic, Y Sentoku, Z-M Sheng, M M Skoric and T Sato,
Stimulated Photon Cascade and Condensate in Relativistic Laser-plasma Interaction Nov 2000

NIFS-670 L Hadzievski, M M Skoric and T Sato,
On Origin and Dynamics of the Discrete NLS Equation Nov 2000

NIFS-671 K Ohkubo, S Kubo, H Idei, T Shimozuma, Y Yoshimura, F Leuterer, M Sato and Y Takita,
Analysis of Oversized Sliding Waveguide by Mode Matching and Multi-Mode Network Theory Dec 2000

NIFS-672 C. Das, S Kida and S Goto,
Overall Self-Similar Decay of Two-Dimensional Tirbulence Dec 2000

NIFS-673 L A Bureyeva, T Kato, V.S. Lisitsa and C Namba,
Quasiclassical Representation of Autoionization Decay Rates in Parabolic Coordinates Dec 2000

NIFS-674 L A Bureyeva, V S Lisitsa and C. Namba,
Radiative Cascade Due to Dielectronic Recombination Dec 2000

NIFS-675 M FHeyn, S V Kasilof, W Kernbichler, K Matsuoka, V V Nemov, S Okamura, O S Pavlichenko,
Configurational Effects on Low Collision Plasma Confinement in CHS Heliotron/Torsatron, Jan 2001

NIFS-676 K. Itoh,
A Prospect at 11th International Toki Conference - Plasma physics, quo vadis?, Jan 2001

NIFS-677 S Satake, H Sugama, M Okamoto and M. Wakatani,
Classification of Particle Orbits near the Magnetic Axis in a Tokamak by Using Constants of Motion, Jan 2001

NIFS-678 M Tanaka and A Yu Grosberg,
Giant Charge Inversion of a Macroion Due to Multivalent Counterions and Monovalent Coions. Molecular Dynamics Studyn, Jan 2001

NIFS-679 K Akaishi, M Nakasuga, H Suzuki, M Iima, N Suzuki A Komori, O Motojima and Vacuum Engineering Group,
Simulation by a Diffusion Model for the Variation of Hydrogen Pressure with Time between Hydrogen Discharge Shots in LHD, Feb. 2001

NIFS-680 A Yoshizawa, N Yokoi, S Nisizima S-I Itoh and K Itoh
Variational Approach to a Turbulent Swirling Pipe Flow with the Aid of Helicity, Feb 2001

NIFS-681 Alexander A Shishkin
Estafette of Drift Resonances, Stochasticity and Control of Particle Motion in a Toroidal Magnetic Trap. Feb 2001

NIFS-682 H Momota and G H Miley,
Virtual Cathode in a Spherical Inertial Electrostatic Confinement Device, Feb 2001

NIFS-683 K Saito, R Kumazawa, T Mutoh, T Seki, T Watari, Y Torii D.A Hartmann, Y Zhao A Fukuyama, F Shimpo, G Nomura, M Yokota, M Sasao, M Isobe, M Osakabe, T Ozaki, K Narihara, Y Nagayama, S Inagaki, K. Itoh, S Morita A V Krasilnikov, K Ohkubo, M Sato, S. Kubo, T Shimozuma, H Idei Y Yoshimura, O Kaneko, Y Takeiri Y Oka, K Tsumori, K Ikeda, A Komori H Yamada, H Funaba, K Y Watanabe, S. Sakakibara, M Shoji, R Sakamoto, J Miyazawa K Tanaka B J Peterson, N Ashikawa, S Murakami, T Minami, S. Ohakachi S Yamamoto, S Kado, H Sasao, H Suzuki K. Kawahata, P deVries, M Emoto, H Nakanishi T Kobuchi, N Inoue, N Ohyabu, Y Nakamura, S Masuzaki, S Muto, K Sato T Morisaki, M Yokoyama, T Watanabe, M. Goto, I Yamada, K Ida T Tokuzawa, N Noda, S Yamaguchi, K Akaishi, A Sagara, K Toi, K Nishimura, K Yamazaki S Sudo Y Hamada, O Motojima, M Fujiwara,
Ion and Electron Heating in ICRF Heating Experiments on LHD Mar 2001

NIFS-684 S Kida and S Goto,
Line Statistics Stretching Rate of Passive Lines in Turbulence Mar 2001

NIFS-685 R Tanaka, T Nakamura and T. Yabe,
Exactly Conservative Semi-Lagrangian Scheme (CIP-CSL) in One-Dimension Mar 2001

NIFS-686 S. Toda and K. Itoh,
Analysis of Structure and Transition of Radial Electric Field in Helical Systems Mar 2001